

# Formation of shock waves in a Bose-Einstein condensate

Bogdan Damski

*Instytut Fizyki, Uniwersytet Jagielloński,  
ul. Reymonta 4, PL-30-059 Kraków, Poland*

and

*Institut für Theoretische Physik,  
Universität Hannover, D-30167 Hannover, Germany*

We consider propagation of density wave packets in a Bose-Einstein condensate. We show that the shape of initially broad, laser-induced, density perturbation changes in the course of free time evolution so that a shock wave front finally forms. Our results are well beyond predictions of commonly used zero-amplitude approach, so they can be useful in extraction of a speed of sound from experimental data. We discuss a simple experimental setup for shock propagation and point out possible limitations of the mean-field approach for description of shock phenomena in a BEC.

PACS numbers: 03.75.Kk,47.35.+i

## I. INTRODUCTION

Spectacular creation of a Bose-Einstein condensate (BEC) in atomic traps [1] has opened unique possibilities for controlled studies of ultracold bosonic gases [2]. One of the basic problems in physics of a BEC is how density perturbations propagate throughout a bosonic cloud. There has been a big interest in this problem and both an experiment [3] and theoretical studies [4, 5] have been performed. These theoretical calculations have been done, however, for infinitesimally small perturbations, which dynamics hardly exhibits nonlinear effects leading to formation of shock waves. This paper is devoted to theoretical studies of a shock wave formation in homogeneous and harmonically trapped BEC.

Shock waves have been widely investigated in different physical systems [6]. For example, we find them in a gas bubble driven acoustically [7], in a photonic crystal [8] and even in mathematical models of traffic flow [6]. Of particular importance are studies of shock waves in classical compressible gases, where they appear whenever large enough density perturbation propagates [9, 10]. Contrary to the case of classical gases, shock waves in ultracold "quantum" atomic gases still require both theoretical and experimental investigations even though some results have been already obtained. The propagation of steep density perturbations in a BEC has been experimentally investigated in [11]; the theory of shocks in Fermi (Tonks) gas has been proposed in [12]; an approximate theoretical description of shock waves in a BEC has been worked out in [13]. It is also worth to mention that shocks have been studied in physical systems governed by nonlinear Schrödinger equation [14, 15]. These studies can be related to investigations of shock waves in a BEC due to formal similarity between the nonlinear Schrödinger equation and mean-field equations of a BEC. Nevertheless, it is important to realize that dynamics of shock waves even in weakly interacting Bose gas, may differ from predictions of the mean-field approximation, as will be proposed in Sec. II.

The mean-field description of a BEC is provided by

the Gross-Pitaevskii equation [16], which in the hydrodynamical variables and dimensionless form [17] reads

$$\begin{aligned} \frac{\partial \rho}{\partial t} + \frac{\partial}{\partial x}(v\rho) &= 0, \\ \frac{\partial v}{\partial t} + \frac{\partial}{\partial x}\left(\frac{1}{2}v^2 + V\right) + \frac{\partial}{\partial x}\left(g\rho - \frac{1}{2}\frac{\partial_x^2 \sqrt{\rho}}{\sqrt{\rho}}\right) &= 0. \end{aligned} \quad (1)$$

First equation is a continuity equation, while the second one is similar to the Euler equation from classical hydrodynamics. Naturally,  $\rho$  is atomic density and  $v$  is a velocity field. The atomic density in (1) satisfies  $\int dx \rho = 1$ , a constant  $g > 0$  is proportional to the strength of two-body repulsive interactions between atoms. The term  $\propto \partial_x^2 \sqrt{\rho}/\sqrt{\rho}$  is called quantum pressure (QP). It is comparable to the  $g\rho$  term only if the spatial scale of density variations is of the order of the healing length  $\xi(\rho)$ . Simple estimation on the basis of (1) shows that  $\xi(\rho) = 1/\sqrt{2g\rho}$ .

In the following we assume that a BEC is initially in a state having a Gaussian-like density wave packet created by adiabatically focused laser beam on an atomic cloud. Alternatively, an atomic cloud can be cooled in a presence of a laser beam, as proposed in [3]. We assume that the width of a laser beam is large compared to the system's healing length, so that the density perturbation is broad and the QP term, at least initially, is negligible. We are interested in dynamics of such a laser-induced perturbation after abrupt laser turn off. We show that it splits into two wave packets propagating in opposite directions. These wave packets undergo self-steepening dynamics. Finally, two shock wave fronts are formed.

## II. 1D HOMOGENEOUS SYSTEMS

First we consider the case of a one-dimensional (1D) BEC in a periodic box having boundaries at  $x = \pm l$ . There is initially a laser beam producing the potential  $V = u_0 \exp(-x^2/2\sigma^2)$  with  $\sigma \ll l$  and  $u_0$  being controlled by intensity and detuning of a laser beam. The initial

density of atoms takes form

$$\rho(x, 0) = \rho_0 + 2\eta\rho_0 e^{-x^2/2\sigma^2}, \quad (2)$$

where  $\rho_0 = 1/(2l + 2\eta\sqrt{2\pi}\sigma)$  provides normalization of (2). We assume that the system is in the ground state which implies  $v(x, 0) = 0$ , and that the QP term is negligible:  $\sigma \gg \xi(\rho_0)$ . It means that we are in the so-called Thomas-Fermi (TF) regime [16]. Under such conditions  $2\eta\rho_0 = -u_0/g$ .

Let us first inspect what happens in a low amplitude limit. The analysis can be done in the framework of a Bogoliubov approach or within a hydrodynamical approach. The first possibility was explored for ultracold fermions in [12]. Here we follow the second one to give the reader more insight into the problem.

We express  $\rho(x, t)$  as  $\rho_0 + \delta\rho(x, t)$  with  $|\delta\rho(x, t)/\rho_0| \ll 1$ . Having in mind that the velocity field  $v(x, t)$  is of the same order as  $\delta\rho(x, t)$ , a linearization of (1) without the QP term gives

$$\begin{aligned} \left( \frac{\partial^2}{\partial t^2} - c_0^2 \frac{\partial^2}{\partial x^2} \right) \phi(x, t) &= 0, \\ v(x, t) = \frac{\partial \phi}{\partial x}, \quad \delta\rho(x, t) &= -\frac{1}{g} \frac{\partial \phi}{\partial t}, \end{aligned} \quad (3)$$

where  $c_0 = \sqrt{g\rho_0}$  is a speed of sound wave propagating on density  $\rho_0$  [18]. Straightforward calculation determines the solution of (3) that satisfies initial conditions  $\delta\rho(x, 0) = 2\eta\rho_0 \exp(-x^2/2\sigma^2)$  and  $v(x, 0) = 0$ :

$$\phi(x, t) = \frac{\eta\rho_0\sigma}{\sqrt{2\pi}} \int dk e^{-k^2\sigma^2/2} g[\sin(kx_+) - \sin(kx_-)]/kc_0,$$

with  $x_{\pm} = x \mp c_0 t$ . Using the explicit form of  $\phi(x, t)$  and (3) we find

$$\delta\rho(x, t) = \eta\rho_0 \left[ e^{-(x-c_0t)^2/2\sigma^2} + e^{-(x+c_0t)^2/2\sigma^2} \right]. \quad (4)$$

Therefore, the initial perturbation splits into two pieces traveling in opposite directions with a speed of sound during free time evolution (Fig. 1a-b). Such a process is impossible in a system which dynamics is governed by a single-particle Schrödinger equation. It is a nice interaction-induced phenomenon in a BEC. Interestingly, a similar effect can be observed in Fermi (Tonks) clouds [12]. It is also easy to see from (3) that the splitting phenomenon happens in exactly the same way regardless of the form of an initial shape.

Let us also remark that, since we consider particles in a periodic box, all the equations should be strictly speaking written in an appropriate Fourier basis. For  $\sigma \ll l$  and  $c_0 t < l$  the discrepancy between obtained results and exact ones is hardly visible.

Even though the solution (4) was derived for small perturbations ( $|\eta| \ll 1$ ) it can be found numerically that the splitting of an initial wave packet into two oppositely moving pieces takes place for  $|\eta| \sim 1$  as well. Quantitative comparison of (4) to exact numerical results reveals

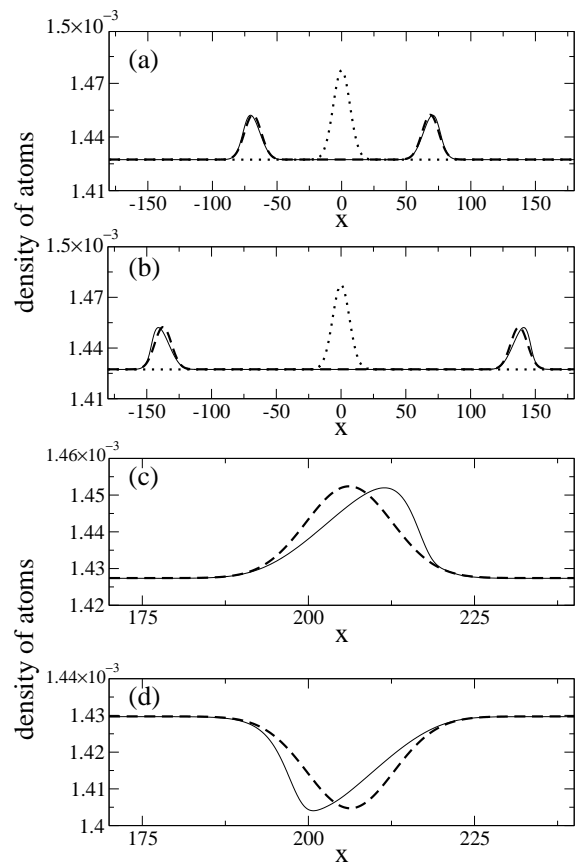


FIG. 1: Density of atoms during free time evolution. Dotted line – an initial density profile, dashed line – the prediction (4), solid line – a numerical solution of (1) with the QP term. Plot (a) [(b)]:  $\eta = 0.0175$  and  $t = 21$  [ $t = 42$ ]. Plot (c) [(d)]: the right-moving wave packet for  $\eta = 0.0175$  [ $\eta = -0.0175$ ] at  $t = 63$ . Other parameters:  $g = 7.5 \cdot 10^3$ ,  $\sigma = 6.5$ ,  $l = 350$ .

discrepancies growing in the course of time evolution for any  $|\eta|$ . An exact solution for  $\eta > 0$  ( $\eta < 0$ ) moves faster (slower) and changes its shape so that the front (back) impulse's edge self-steepens – Fig. 1c-d.

To explain that behavior we have found, following [9], the exact traveling wave solution of Eqs. (1) without the QP term:

$$\rho = f(x - (a_0 \pm 3\sqrt{g\rho})t) \quad , \quad v = a_0 \pm 2\sqrt{g\rho}, \quad (5)$$

where  $f$  (an arbitrary function) and  $a_0$  (a constant) can be determined from initial conditions. The sign  $\pm$  determines a direction of propagation. The result (5) is valid as long as a spatial scale of density perturbations is larger than the healing length  $\xi$ . Solutions of the form (5) were previously worked out in various physical systems, see e. g. [13, 14, 15].

Nonlinearity of (1) prevents usage of the superposition principle to build a solution, that contains both left and right-moving perturbations, out of (5). Fortunately, the problem can be simplified, since after separation perturbations move independently.

We propose to consider only the right-moving ( $r$ ) part and to take as an initial density profile  $\rho_r(x, 0) = \rho_0 + \rho_0 \eta e^{-x^2/2\sigma^2}$  (compare (2)). Such an approximation is exact for small perturbations and turns out to be good for large ones – see discussion of numerical simulations presented below. The constant  $a_0$  is found to be  $-2\sqrt{g\rho_0}$  from a requirement that initially the velocity field far from the perturbation is zero:  $v(x \rightarrow \pm l, 0) = 0$ . This assumption leads to the solution

$$\rho_r(x, t) = \rho_0 + \rho_0 \eta \exp(-[x - \sqrt{g}(-2\sqrt{\rho_0} + 3\sqrt{\rho_r})t]^2/2\sigma^2). \quad (6)$$

Although (6) is in an implicit form, all the quantities characterizing a shock wave formation can be analytically extracted from it.

Both amplitude and velocity of impulse's maximum are constant during time evolution. The amplitude equals  $\rho_0(1 + \eta)$ , while the velocity becomes  $\mathcal{V}(\eta) = \sqrt{g\rho_0}\mathcal{A}(\eta)$  where

$$\mathcal{A}(\eta) = 3\sqrt{1 + \eta} - 2. \quad (7)$$

For small perturbations we get  $\mathcal{V}(\eta) = \sqrt{g\rho_0}(1 + 3\eta/2)$ . Taking  $\eta = 0$  we find a well known expression for a sound velocity:  $\sqrt{g\rho_0}$  [18]. These results show explicitly that bright perturbations ( $\eta > 0$ ) move faster than dark ones ( $\eta < 0$ ). A typical measurement of a sound velocity relies on observation of propagation of density perturbations on a cloud [3]. If such perturbations are not small enough our results indicate that the  $\eta$  dependent term in  $\mathcal{V}(\eta)$  has to be considered in the experimental determination of a sound velocity.

For clarity of discussion we will concentrate now on *bright perturbations*. A speed of impulse's maximum is bigger than a speed of its tails. As a result an impulse self-steepens in the direction of propagation so that formation of a shock wave front takes place. Finally,  $\partial_x \rho_r(x, t_s) = -\infty$  at  $x = x_s$  leading to the well known wave breaking phenomenon [6].

Time required for such a process ( $t_s$ ) can be estimated as follows: the impulse's half-width ( $\approx 2\sigma$ ) is a difference in distance traveled by lower and upper impulse's parts until the shock appears:  $(\mathcal{V}(\eta) - \mathcal{V}(0))t_s \approx 2\sigma$ . It gives

$$t_s \approx \frac{2\sigma}{3(\sqrt{1 + \eta} - 1)\sqrt{g\rho_0}}. \quad (8)$$

Quantitatively time of shock creation and shocks' position can be determined from a set of equations [9]

$$\frac{\partial x(\rho_r)}{\partial \rho_r} = 0, \quad \frac{\partial^2 x(\rho_r)}{\partial \rho_r^2} = 0. \quad (9)$$

The first one says that  $\partial_x \rho_r$  is infinite, while the second one assures uniqueness of the  $\rho_r(x, t_s)$  function. Assuming  $\eta > 0$  we find that

$$x(\rho_r) = \sqrt{g}(-2\sqrt{\rho_0} + 3\sqrt{\rho_r})t + \sqrt{-2\sigma^2 \ln[(\rho_r/\rho_0 - 1)/\eta]}, \quad (10)$$

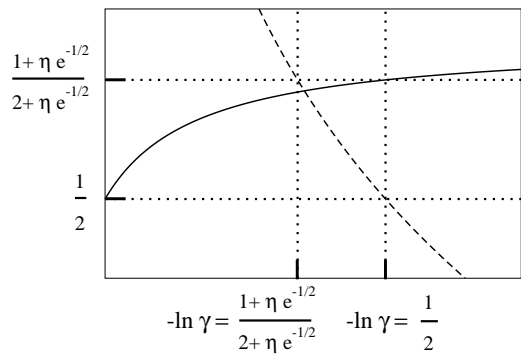


FIG. 2: Schematic plot of functions:  $-\ln \gamma$  (dashed line) and  $(1 + \eta\gamma)/(2 + \eta\gamma)$  (solid line) vs.  $\gamma$ . Dotted lines define bounds leading to inequalities (13).

which substituted into (9) leads to

$$t_s = \frac{\sqrt{2}\sigma \sqrt{\rho_s + \rho_0}}{3\sqrt{g} \rho_s - \rho_0}, \quad (11)$$

where  $\rho_s$ , the density at which  $\partial_x \rho_r = -\infty$ , satisfies

$$-\ln[(\rho_s/\rho_0 - 1)/\eta] = \frac{\rho_s}{\rho_s + \rho_0}. \quad (12)$$

It seems to be impossible to solve analytically that equation. Fortunately, its numerical treatment is straightforward. It is possible, however, to prove analytically that the solution of (12) exists and satisfies the relation

$$\rho_0 + \rho_0 \eta e^{-\mathcal{B}(\eta)} \leq \rho_s \leq \rho_0 + \rho_0 \eta e^{-1/2}, \quad (13)$$

where

$$\mathcal{B}(\eta) = \frac{1 + \eta e^{-1/2}}{2 + \eta e^{-1/2}}.$$

For  $\eta \rightarrow 0$  lower and upper bounds coincide. One can derive inequalities (13) by means of a graphical method – Fig. 2. Let us introduce a variable  $0 \leq \gamma \leq 1$  such that  $\rho_s = \rho_0(1 + \eta\gamma)$ . Eq. (12) now takes the form:  $-\ln \gamma = (1 + \eta\gamma)/(2 + \eta\gamma)$ . The RHS of this equation increases monotonically with  $\gamma$  from  $1/2$  to  $(1 + \eta)/(2 + \eta)$ . Conversely, the LHS decreases monotonically with  $\gamma$  from  $+\infty$  to  $0$ . Therefore there must be  $\gamma$  at which the RHS equals the LHS. For  $\gamma > \exp(-1/2)$  the LHS becomes smaller than  $1/2$ . It means that  $\gamma \leq \exp(-1/2)$  in the considered problem. Therefore, the RHS takes the highest value for  $\gamma = \exp(-1/2)$ , so it is bounded from above by  $\mathcal{B}(\eta)$ . As a result, we arrive at a conclusion that the solution exists and  $1/2 \leq -\ln \gamma \leq \mathcal{B}(\eta)$  leading to inequalities (13).

On the basis of (11) and (13) we have found bounds for time of shock formation

$$t_s \leq \frac{\sqrt{2}\sigma e^{\mathcal{B}(\eta)}}{3\eta\sqrt{g\rho_0}} \sqrt{2 + \eta e^{-\mathcal{B}(\eta)}}, \quad (14)$$

$$t_s \geq \frac{\sqrt{2}\sigma e^{1/2}}{3\eta\sqrt{g\rho_0}} \sqrt{2 + \eta e^{-1/2}}.$$

In the  $\eta \rightarrow 0$  limit both bounds equal  $2\sigma e^{1/2}/3\eta\sqrt{g\rho_0}$ . From inequalities (14) we see that the shock appears if a wave packet evolves long enough. This observation together with the explicit expression for a speed of propagation of density maximum is a central result of this paper. Considerations (3)-(4) fail to predict such behavior since they are valid in the  $\eta \rightarrow 0$  limit where  $t_s \rightarrow \infty$ . As mentioned above these calculations have been done for bright wave packets ( $\eta > 0$ ). Extension to dark impulses is straightforward. We would like also to point out that the solution (6) is uniquely defined in a whole space up to the time of shock creation, i.e. for  $t \leq t_s$  – see Fig. 4b and Ref. [19]. Later on, the solution (6) in a shock wave front region becomes multi-valued, compare [13, 14, 15].

Approximating the position of a shock wave front by position of impulse's maximum at  $t = t_s$ :  $x_s = \mathcal{V}(\eta)t_s$ , we get

$$\begin{aligned} x_s &\leq \frac{\sqrt{2}\sigma e^{\mathcal{B}(\eta)}}{3\eta} \sqrt{2 + \eta e^{-\mathcal{B}(\eta)}} \mathcal{A}(\eta), \\ x_s &\geq \frac{\sqrt{2}\sigma e^{1/2}}{3\eta} \sqrt{2 + \eta e^{-1/2}} \mathcal{A}(\eta). \end{aligned} \quad (15)$$

As  $\eta \rightarrow 0$  we have  $x_s \rightarrow 2\sigma e^{1/2}/3\eta$ .

Let us compare numerical simulations of hydrodynamical equations with the QP term to above derived analytical predictions. We must be aware that analytical calculations have been performed without taking the QP term into account. Initially a spatial scale of density variations is roughly  $\sigma$ , which is much greater than the healing length  $\xi$ . As a result the QP term is negligible at the beginning of time evolution. As shocks form up density changes occur on smaller and smaller length scales being finally of the order of  $\xi$ . Therefore, before appearance of shocks quantum pressure has to start to play a role leading to discrepancy between analytical predictions and numerical simulations.

For numerical purposes, we have fixed the dimensionless coupling constant  $g$  to  $7.5 \cdot 10^3$ . In a typical 3D configuration such a value corresponds to roughly  $10^5 \sim 10^6$  atoms of either  $^{87}\text{Rb}$  or  $^{23}\text{Na}$ . In the present calculations such a value of  $g$  guarantees that we are well in the Thomas-Fermi regime, which is important for discussed phenomena. The same qualitative results were obtained for  $g$  in the range  $2 \cdot 10^3 - 5 \cdot 10^4$ .

We have performed numerically time evolutions and have observed density wave packets until they reached box boundaries being at  $x = \pm l$ . These results can be divided into two groups: the case of  $x_s > l$  and that of  $x_s < l$ . In the first situation we do not observe shocks, although a shock-like deformation of an impulse's shape can be clearly visible. The agreement between analytical solution (6) and full numerical simulation is very good – Fig. 3. When  $x_s < l$  shocks appear. A typical situation is depicted in Fig. 4a-c.

First of all, as a relative height of a wave packet grows, amplitude of separated density perturbations becomes a little bit smaller than half-amplitude of an initial pertur-

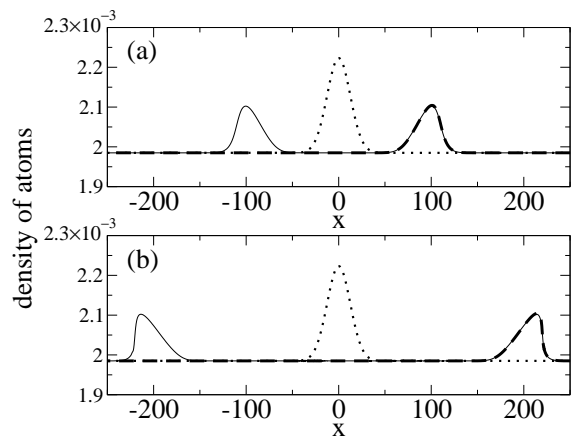


FIG. 3: Density of atoms during free time evolution. Dotted line – an initial density of atoms, dashed line – the analytical solution (6), solid line – a numerical solution of Eq. (1) with the QP term. Plot (a) [(b)] is for  $t = 24$  [ $t = 51$ ]. Other parameters:  $\eta = 0.06$ ,  $t_s = 60.4$ ,  $x_s = 253.8$ ,  $g = 7.5 \cdot 10^3$ ,  $\sigma = 12.5$ ,  $l = 250$ .

bation. It leads to a small discrepancy between analytical predictions and numerics (Fig. 4a).

Second, a slope of the impulse does not become infinite at  $t = t_s$ , but significantly increases. To express it quantitatively we have defined a relative slope by

$$\Xi(t) = \frac{\max(-\frac{\partial \rho(x,t)}{\partial x})}{\frac{\eta \rho_0}{\sigma} e^{-1/2}}, \quad (16)$$

where the denominator is  $\max(-\frac{\partial \rho}{\partial x})$  for a single wave packet which density is  $\rho_0 + \eta \rho_0 \exp(-x^2/2\sigma^2)$ . After the splitting  $\Xi \approx 1$  and then grows. As depicted in Fig. 4c the relative slope can be as large as few tens showing that a shock formation occurs on a time scale  $t \sim t_s$ .

Third, for  $t > t_s$  density oscillations in the mean-field approach with the QP term show up instead of a true shock wave front. As shown in Fig. 4b, for  $t > t_s$  the analytical solution (6) still fits to numerics, but in a back edge of an impulse *only*. In the front part the solution (6) becomes multi-valued, as expected from the theory of nonlinear equations [6, 19]. We have checked that the appearance of density oscillations is a result of coming into play of the QP term. It is not an artifact of inability of our numerical methods to evolve a truly shock wave front if such would appear [20]. Qualitatively the same results were obtained by other means in [13, 14, 15].

Similar density oscillations have been recently observed in a paper that describes shock wave formation in a Fermi (Tonks) cloud [12]. We have shown there that they are an artifact of the usage of the mean-field approximation. Indeed, they were absent in exact many-body calculations. In a Fermi (Tonks) cloud there were three stages of shock dynamics: a shock wave formation, propagation of a shock-like impulse roughly without change of shape, and impulse's explosion leading to broadening of density profile. The mean-field approach has reproduced only

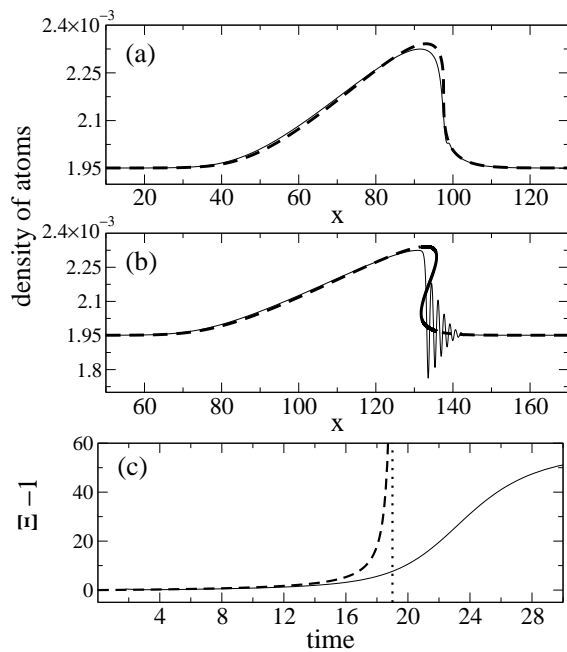


FIG. 4: Plots (a) and (b): density profile of the right-moving wave packet. Dashed line – the analytical solution (6), solid line – a solution of (1) with the QP term, thick solid line in (b) shows multi-valued part of the solution (6). Plot (a) [(b)] is for  $t = 18.9$  [ $t = 27$ ]. Plot (c): relative slope (16) of the right-moving wave packet. Dotted line indicates time of shock formation (11)-(12). Parameters:  $\eta = 0.2$ ,  $\sigma = 12.5$ ,  $t_s = 19$ ,  $x_s = 93.5$ ,  $g = 7.5 \cdot 10^3$ ,  $l = 250$ ,  $\xi(2 \cdot 10^{-3}) = 0.18$ .

the first stage. The second stage was absent – density oscillations have appeared in the same way as here. As a result, we speculate, that it is rather doubtful that predictions of the Gross-Pitaevskii equation at the front edge are reliable after appearance of density modulations.

It is difficult to make any definite statements about applicability of the Gross-Pitaevskii equation for description of shocks without the insight into a many-body theory of interacting bosons. To understand the possible source of problems we recall that the N-body bosonic wave function has a general form:

$$\sqrt{\lambda_0} \phi(x_1) \cdots \phi(x_N) + \text{an orthogonal part.}$$

The condensate fraction  $\lambda_0 \in (0, 1]$  is divided by  $N$  the highest eigenvalue of a single particle density matrix.  $\phi(x)$  is the eigenvector of that matrix to eigenvalue  $\lambda_0$ . In the mean-field approach we assume  $\lambda_0 \approx 1$ . Nevertheless,  $\lambda_0$  can change during time evolution. In principle, it can be noticeably lower than one after a shock creation. It means that contribution of states orthogonal to a condensate mode, neglected in a mean-field treatment, might be significant. These states may smooth density changes by filling the oscillatory region with atoms depleted from a condensate. Similar situation one encounters for dark soliton in a BEC [23], namely a soliton's notch, which size is also of the order of the healing length, fills with depleted atoms.

### III. 1D HARMONICALLY TRAPPED SYSTEMS

Now we would like to find out what happens if an external harmonic trapping potential is imposed on a 1D bosonic cloud. Atoms are initially placed in both harmonic and laser potentials [17]

$$V = \frac{x^2}{2} + u_0 \exp(-x^2/2\sigma^2).$$

The atomic density, in the TF limit, takes form

$$\rho(x, 0) = \frac{\mu}{g} - \frac{x^2}{2g} - \frac{u_0}{g} e^{-x^2/2\sigma^2}, \quad (17)$$

for  $|x| \leq R_{TF} = \sqrt{2\mu}$  and zero for  $|x| > R_{TF}$ . Similarly as before, relative amplitude  $2\eta$  of an initial perturbation is defined by relation  $2\eta\mu/g = -u_0/g$ . We have restricted our numerical simulations to bright perturbations in this section:  $\eta > 0$ . We have also assumed that the width of a laser beam is much smaller than spatial extent of the cloud. Under these conditions the chemical potential  $\mu$ , found from the normalization of (17), equals

$$\mu(u_0) = [(1 + u_0\sqrt{2\pi}\sigma/g)3g/4\sqrt{2}]^{2/3}. \quad (18)$$

Once again, we are interested in dynamics of Gaussian-like wave packets created after an abrupt laser turn off.

First of all, a splitting of an initial perturbation into two propagating outward pieces takes place regardless of an initial position of a density perturbation. Secondly, there appears self-steepening of the bright (dark) impulse's front (back) edge – see Fig. 5a. Finally, density oscillations appear showing that an impulse enters a shock regime.

We were unable to find exact solutions of Eqs. (1) in a trapped case even when the QP term was absent. Instead of it, we can provide a simple semi-analytical prediction for a speed of density perturbations on the cloud. To this aim we add  $x^2/2g$  term to the density of atoms  $\rho(x, t)$ . Such a transformation removes a harmonic trapping term in (17) and propagation of impulses is qualitatively similar to the homogeneous case carefully discussed above (Fig. 5b). Depending on amplitude of outward moving perturbations, in the  $\rho(x, t) + x^2/2g$  picture, impulses' amplitude can change a little during propagation. Therefore, it is not easy to find out phenomenologically a simple rule that governs motion of Gaussian-like wave-packets in a harmonically trapped system.

We have tried different semi-analytical formulas for the prediction of a position of a wave packet's maximum, and found that the following approach is the most accurate. In a homogeneous case a speed of a density perturbation was greater than a local sound velocity by the factor  $\mathcal{A}(\eta)$  (7), with  $\eta$  being a relative impulse's amplitude (6). We have assumed that a similar law holds also now. It leads to the following approximate equation for the position of a maximum of  $\rho(x, t) + x^2/2g$

$$\frac{dx_m}{dt} \approx \mathcal{A}(\eta) \sqrt{\mu - x_m^2/2}. \quad (19)$$

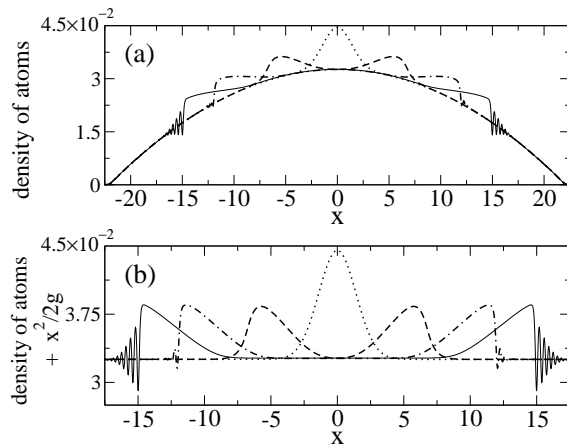


FIG. 5: Plot (a): density of atoms at different time moments. Plot (b): the same as in the plot (a) but with the  $x^2/2g$  term added to the density profile in order to remove a trivial position dependence of atomic density due to external harmonic trapping potential – see Eq. (17). Dotted line –  $t = 0$ , dashed line –  $t = 0.3$ , dashed-dotted –  $t = 0.6$ , solid line –  $t = 0.8$ . Both  $t$  and  $x$  are expressed in harmonic oscillator units [17]. Other parameters:  $u_0 = -90$ ,  $\eta = 0.184$ ,  $g = 7.5 \cdot 10^3$ ,  $\sigma = 1.4$ ,  $R_{TF} \approx 22$ .

Integrating (19) we have found

$$x_m(t, \eta) = R_{TF} \sin\left(\frac{\mathcal{A}(\eta)\sqrt{\mu}}{R_{TF}}t\right). \quad (20)$$

In the limit of  $\eta \rightarrow 0$  the zero-amplitude result of [4] is recovered. We have checked prediction (20) for  $\eta$  as large as 0.4 and  $g = 7.5 \cdot 10^3$ . Notice that it corresponds to relative amplitude of an initial perturbation equal to 80%! Numerical results are depicted in Fig. 6a-c. As easily noticed, the agreement between numerics and the formula (20) is satisfactory. We have observed that as  $x_m \rightarrow R_{TF}$ , Eq. (20) underestimates slightly a position of impulse's maximum for small  $\eta$  and overestimates exact result for large  $\eta$  [22]. For  $\eta \approx 0.18$  the agreement between numerics and semi-analytics is excellent – Fig. 6b. Despite differences far away from a trap center it is important to notice that the formula (20) correctly works near a trap center, where density is quite homogeneous. Indeed, Eq. (20) reproduces nicely numerics at least for  $x_m(t, \eta) \leq R_{TF}/2$ ,  $\eta \in (0.02, 0.4)$ , and other parameters as in the caption of Fig. 6.

On the basis of (20) we conclude that near a trap center, where  $R_{TF} \sin(\mathcal{A}(\eta)\sqrt{\mu}t/R_{TF}) \approx \mathcal{A}(\eta)\sqrt{\mu}t$ , the position of impulse's maximum changes linearly in time and its speed of propagation equals  $\mathcal{A}(\eta)\sqrt{\mu}$ . This observation is in qualitative agreement with the experiment performed in a quasi-one-dimensional configuration [3]. The most important message from the formula (20) is that the speed of finite size wave packets can differ significantly from the zero-amplitude result by the factor  $\mathcal{A}(\eta)$ . For a realistic value of  $\eta = 0.3$  a speed of a wave packet's maximum is greater from the zero-amplitude prediction

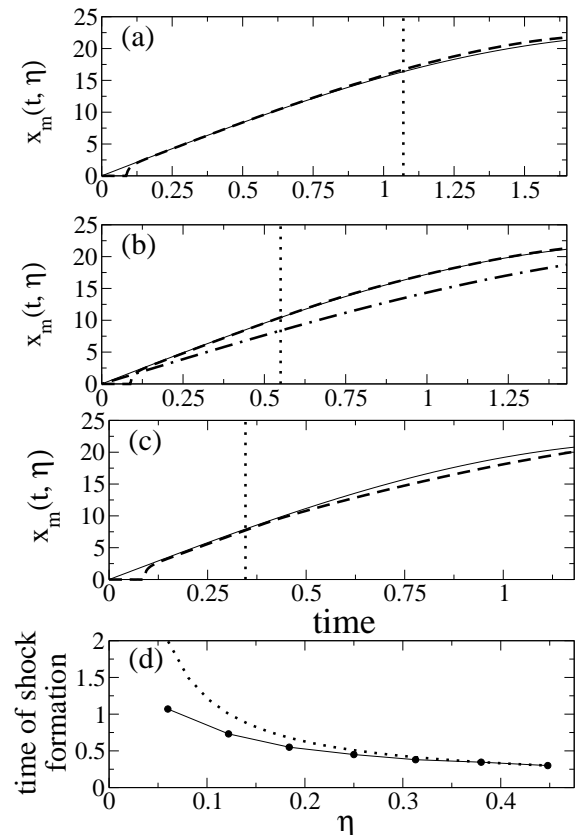


FIG. 6: Plots (a)-(c): a position of impulse's maximum vs. time. Solid line – the semi-analytical prediction (20), dashed line – numerics on the basis of (1) with the QP term, dotted line – time of shock formation extracted from numerics (see text). Dashed-dotted line on the plot (b):  $x_m(t, 0)$ . Parameters  $(u_0, \eta)$  for plots (a)-(c):  $(-30, 0.06)$ ,  $(-90, 0.184)$ ,  $(-180, 0.39)$ , respectively. Plot (d): time of shock formation vs. relative amplitude of an impulse. Solid line comes from numerics, while dotted line is an approximation (21). Both  $t$  and  $x$  are expressed in harmonic oscillator units [17]. Other parameters:  $g = 7.5 \cdot 10^3$ ,  $\sigma = 1.4$ ,  $R_{TF} \approx 22$ .

by more than 40%! We would like to stress, however, that these estimations are obtained for idealized case of a one-dimensional BEC, while the real experiments are typically performed in quasi-one-dimensional setups. Further studies are needless for clarification of whether similarly strong dependence of the speed of finite size wave packets on their amplitude survives in a quasi-one-dimensional configurations similar to that of [3]. The propagation of tiny density perturbations in harmonically trapped quasi-one-dimensional setups was discussed in [4, 5]. These papers show that the tight confinement in cigar-shaped configurations changes the sound velocity expected for one-dimensional harmonically trapped systems by a factor  $1/\sqrt{2}$ . If the same property would hold for finite density perturbations, the application of our results from this section to quasi-one-dimensional systems would be straightforward.

From our simulations we have extracted time of shock

formation, defined now by a time moment when density oscillations in a shock front have amplitude large enough to lower density  $\rho(x) + x^2/2g$  below the background value  $\mu/g$ . We have found that shock-like behavior shows up for any  $\eta \in (0.06, 0.45)$  and other parameters as in the caption of Fig. 6. The shock behavior of a large wave packet takes place in a relatively homogeneous part of the cloud where a sound velocity is  $\approx \sqrt{\mu}$ . Replacing in the formula (8)  $\sqrt{g\rho_0}$  by  $\sqrt{\mu}$  the following estimation for time of shock creation can be derived

$$t_s \approx \frac{2\sigma}{3(\sqrt{1+\eta}-1)\sqrt{\mu}}. \quad (21)$$

As depicted in Fig. 6d, this semi-analytical formula nicely reproduces time of a shock formation for large enough  $\eta$ , and parameters of Fig. 6, despite its approximate character. The same good agreement is found for  $g = 10^4$  and  $g = 1.25 \cdot 10^4$ . For  $g$  lower than  $7.5 \cdot 10^3$ , the case presented on the plot, discrepancy between estimation (21) and exact calculation grows up, e.g. (21) overestimates time of shock formation at  $\eta = 0.4$  and  $g = 2.5 \cdot 10^3$  by about 10%.

#### IV. CONCLUSIONS

We have considered propagation of broad density perturbations in a BEC. Our theoretical approach fully accounts for nonlinear effects in sound propagation so it is well beyond the common zero-amplitude approximation [4, 5], and allows for description of shock formation. As a result, quantitative predictions concerning propagation of large density perturbations in a homogeneous system were given. Extension of these results to harmonically trapped problems resulted in a semi-analytical description in a satisfactory agreement with numerics.

We have focused on 1D systems recently realized experimentally [24], but we expect that our work may provide a theoretical basis for investigations of quasi-one-dimensional setups widely studied in laboratories. The easiest for experimental inspection are predictions for harmonically trapped condensates. We expect that also findings for homogeneous bosonic clouds can be verified with the help of, e. g. atomic wave guides [25].

It is worth to point out that shock-like structures have been already studied experimentally in a two component BEC [11], where time evolution of dark narrow density perturbations was observed. The initial size of a wave packet in [11] was of the order of the healing length, which made observation of impulse's self-steepening, a clear signature that shock formation takes place, very difficult. We expect that the experimental setup proposed by us should give more convincing results. In fact, it seems that a slight change in a setup of [3] together with a little bit higher measurement accuracy should verify our predictions at least qualitatively.

From the theoretical side we would like to note that formation of shock-like solutions in a harmonic trap has

been noticed in [4]. Our considerations provide an analytical insight into their numerics. It is also worth to mention, that it is possible to find an approximate analytical solution of hydrodynamical equations (1) with the quantum pressure term. That solution also exhibits shock behavior, and its properties have been discussed in [13, 14, 15].

It is also interesting to discuss differences between the traveling wave solutions presented in this paper and recently investigated, both theoretically and experimentally, solitonic solutions in a BEC [26]. Our paper describes density perturbations which change their shape during time evolution, while soliton-like density wave packets propagate in dispersionless manner [19]. The main difference between time evolution of wave packets considered here and solitonic ones results mainly from the difference in their width. The width of a soliton is of the order of the healing length, which makes the quantum pressure term in Eq. (1) considerable. This allows for finding a solution that propagate without changes of shape. Our solution, Eq. (5), describes a perturbation that is much broader than the healing length. In this case the quantum pressure term is negligible and instead of solitonic solutions shock waves show up. It is also worth to realize that the initial shape of a shock-like solution, determined by the function  $f(x)$  in Eq. (5), can be arbitrary as long as  $f(x)$  changes significantly on length scales much larger than the healing length. Conversely, solitons have precisely defined shape [19].

One of the main open questions is how the shock-like impulse's front evolves in time. We have pointed out that the mean-field approach gives rather doubtful answer and suggested a possible explanation. Further investigations to resolve that issue will be a subject of future studies. Unfortunately, contrary to the case of Fermi (Tonks) gases [12], it is very difficult to solve a many-body problem exactly.

Finally, it is worth to point out that both a splitting of an initial perturbation and a shock wave formation take place in classical hydrodynamics [10]. It suggests that qualitatively the same phenomena can be observed in a cold bosonic (fermionic) gas above the condensation (Fermi) temperature. The crossover from a classical non-degenerate to a quantum degenerate regime can be an interesting subject for future experimental and theoretical investigations. In particular, differences in properties of cold bosons and fermions can be very exciting. Indeed, e. g. a sound velocity of 1D ultracold bosons (fermions) is  $\sim \sqrt{\rho}$  ( $\sim \rho$ ), while in the non-degenerate regime it has to have the same dependence on density for bosons and fermions.

I would like to acknowledge discussions with Aneta Damska and Zbyszek Karkuszewski. I am also grateful to Andreas Buchleitner for drawing my attention to Ref. [10] and for his hospitality during preparation of the manuscript at MPIPKS Dresden. I want also to thank L. P. Pitaevskii for showing me the Ref. [14]. This work was mainly supported by KBN project 2 P03B 124 22.

Additional support from the Alexander von Humboldt Foundation, Deutsche Forschungsgemeinschaft and VolkswagenStiftung under the grant "Entanglement measures

and the influence of noise" is also gratefully acknowledged.

- 
- [1] M. H. Anderson, J. R. Ensher, M. R. Matthews, C. E. Wieman, and E. A. Cornell, *Science* **269**, 198 (1995).
- [2] J. R. Anglin and W. Ketterle, *Nature* **416**, 211 (2002).
- [3] M. R. Andrews, D. M. Kurn, H. J. Miesner, D. S. Durfee, C. G. Townsend, S. Inouye, and W. Ketterle, *Phys. Rev. Lett.* **79**, 553 (1997); M. R. Andrews *et al.*, *Phys. Rev. Lett.* **80**, 2967 (1998).
- [4] G. M. Kavoulakis and C. J. Pethick, *Phys. Rev. A* **58**, 1563 (1998).
- [5] S. Stringari, *Phys. Rev. A* **58**, 2385 (1998); E. Zaremba, *Phys. Rev. A* **57**, 518 (1998).
- [6] G. B. Whitham, *Linear and Nonlinear Waves* (John Wiley & Sons 1974).
- [7] M. P. Brenner, S. Hilgenfeld, and D. Lohse, *Rev. Mod. Phys.* **74**, 425 (2002).
- [8] E. J. Reed, M. Soljačić, and J. D. Joannopoulos, *Phys. Rev. Lett.* **90**, 203904 (2003);
- [9] L. D. Landau and E. M. Lifshitz, *Fluid Mechanics* (Pergamon 1989). The traveling wave solutions of the form (5) and conditions for a shock formation (9) are discussed in § 101.
- [10] A. J. Sommerfeld, *Mechanik der deformierbaren Medien* (Leipzig 1964).
- [11] Z. Dutton, M. Budde, C. Slowe, and L. V. Hau, *Science* **293**, 663 (2001).
- [12] B. Damski, *J. Phys. B* **37**, L85 (2004).
- [13] A. M. Kamchatnov, A. Gammal, and R. A. Kraenkel, e-print cond-mat/0310457.
- [14] A. V. Gurevich and A. L. Krylov, *Sov. Phys. JETP* **65**, 944 (1987).
- [15] A. M. Kamchatnov, R. A. Kraenkel, and B. A. Umarov, *Phys. Rev. E* **66**, 036609 (2002).
- [16] F. Dalfovo, S. Giorgini, L. P. Pitaevskii, and S. Stringari, *Rev. Mod. Phys.* **71**, 463 (1999).
- [17] Let  $m$  be a mass of a bosonic particle. For a case of particles in a box we take arbitrary length scale  $l_0$  for a unit of length and  $ml_0^2/\hbar$  for a unit of time. In a harmonically trapped system a unit of length equals  $\sqrt{\hbar/m\omega}$  and a unit of time is  $1/\omega$  ( $\omega$  is a harmonic trapping frequency).
- [18] By a sound velocity we understand a speed of propagation of infinitesimally small density perturbations.
- [19] P. G. Drazin and R. S. Johnson, *Solitons: an introduction* (Cambridge University Press 1989).
- [20] We use the Bulirsch-Stoer method [21] in a grid basis for integration of Eqs. (1). Such an approach can not correctly describe shock propagation since it calculates derivatives across a shock wave front. We have performed numerical simulations of (1) without and with the QP term. In the first case the method produced results not converging on arbitrarily large grid – as expected from (6)-(15) shocks have appeared in the numerical solution. Conversely, the results of calculations with the QP term where perfectly converged indicating that shocks were absent in the solution of (1) with the QP term. We have also performed the same calculation in the appropriately truncated Fourier basis to avoid potential problems with calculation of derivatives. As expected, the results were the same as those obtained on a grid for large enough size of the Fourier basis.
- [21] W. H. Press, B. P. Flannery, S. A. Teukolsky, and W. T. Vetterling, *Numerical Recipes* (Cambridge University Press 1987).
- [22] The same qualitative results are obtained for  $g$  in the range  $2.5 \cdot 10^3 - 1.25 \cdot 10^4$ .
- [23] J. Dziarmaga, Z. P. Karkuszewski, and K. Sacha, *Phys. Rev. A* **66**, 043615 (2002); J. Dziarmaga, Z. P. Karkuszewski, and K. Sacha, *J. Phys. B* **36**, 1217 (2003).
- [24] A. Görlitz *et al.*, *Phys. Rev. Lett.* **87**, 130402 (2001).
- [25] A. E. Leanhardt *et al.*, *Phys. Rev. Lett.* **89**, 040401 (2002).
- [26] A. D. Jackson, G. M. Kavoulakis, and C. J. Pethick, *Phys. Rev. A* **58**, 2417 (1998); S. Burger *et al.*, *Phys. Rev. Lett.* **83**, 5198 (1999); J. Denschlag *et al.*, *Science* **287**, 97 (2000); L. Khaykovich *et al.*, *Science* **296**, 1290 (2002); K. E. Strecker, G. B. Partridge, A. G. Truscott, and R. G. Hulet, *Nature* **417**, 150 (2002).